Available online at www.sciencedirect.com
SCIENCE DIRECT
Journal of Molecular Catalysis A: Chemical 238 (2005) 78–87
JOURNAL OF MOLECULAR CATALYSIS A: CHEMICAL
www.elsevier.com/locate/molcata

Studies on gold nanoparticles supported on iron, cobalt, manganese, and cerium oxide catalytic materials

Deepak B Akolekar [a,*], Suresh K Bhargava [a,*], Garry Foran [b], Masashi Takahashi [c]

[a] *Catalysis and Advanced Materials Research Group, Department of Applied Chemistry, RMIT University, City Campus, Melbourne, Vic. 3001, Australia*
[b] *Australian Synchrotron Research Program, c/o ANSTO, PMB 1, Menai, NSW 2234, Australia*
[c] *Department of Chemistry, Toho University, Miyama, Funabashi, Chiba 274-8510, Japan*

Received 21 February 2005; received in revised form 28 April 2005; accepted 28 April 2005
Available online 17 June 2005

Abstract

Gold nanoparticles containing iron, cobalt, manganese, and cerium materials were prepared using precipitation–deposition/co-precipitation methods. The techniques employed for the characterization of these materials were ICP-MS, TGA, TEM, XRD, BET, Mössbauer, and XAS. Au L_3-edge X-ray absorption spectroscopic measurements were carried out over a series of transition and rare earth materials containing gold nanoparticles. The size of gold nanoparticles varied in the range of ∼3 to 7 nm in the Fe/Co/Mn/Ce materials. These materials possess medium between 34 and 63 m^2/g. The XRD analysis of the samples indicated the high phase purity and crystallinity of the support (Fe/Co/Mn/Ce) materials. Mössbauer spectroscopy was employed to obtain valuable information on the electronic and crystallographic structure of gold nanoparticles. An X-ray absorption fine structure (XANES, EXAFS) technique was used in obtaining critical information about the atomic distances, bonding, and neighbouring environment for gold atoms in the Fe/Co/Mn/Ce materials. XAFS and in situ high temperature XRD techniques were used to investigate the influence of the high temperature treatment on gold nanoparticles inside the metal oxide materials. The results obtained from XAFS, XANES, XRD, and Mössbauer analysis confirm the typical characteristics and structure of gold nanoparticles in these materials.

Keywords: Gold nanoparticles; Transition metal oxide; EXAFS; Gold Mössbauer; In situ high temperature XRD; Surface properties

1. Introduction

Nano-structured materials are of great interest in catalytic as well as in speciality electronic applications. Since the development of nanoparticles, research on the synthesis and stabilisation of metal gold particles has undergone rapid expansion. It is well known that nanoparticles find a variety of applications in catalytic material, from sensor to digital data storage, and nano-electromechanical systems, etc. Applications of gold nanoparticles now include biological markers, sensors, molecular recognition systems, catalysis, and nanoscale electronics. Investigations on various nanoparticles and their stabilisation in different matrices are very important and critical in such applications. Information regarding the structures and environment of nanoparticles is very important for nanoparticle selection. Nanoparticles used in different applications rely for their function on different properties [1–3].

Research work [4–7] on gold catalysts has proved that the supported gold systems can be usually active and selective for number of reactions (oxidation/hydrogenation/hydrochlorination, etc.) provided that gold particles are in a particular form/environment/size and distribution. Gold nanoparticles exhibits a unique catalytic nature and action when deposited on a variety of metal oxides. Most reactions are noticeably structure sensitive over supported gold catalysts. Supported gold catalysts are typically used in the

* Corresponding authors. Tel.: +61 399252121/3365; fax: +61 3 96391321.
E-mail addresses: E04781@ems.rmit.edu.au (D.B. Akolekar), Suresh.Bhargava@rmit.edu.au (S.K. Bhargava).

1381-1169/$ – see front matter © 2005 Elsevier B.V. All rights reserved.
doi:10.1016/j.molcata.2005.04.065

low-temperature, catalytic combustion, and partial oxidation of hydrocarbons, CO, hydrogenation of carbon oxides, and unsaturated hydrocarbons reduction of NO, etc. [4–8]. High-resolution X-ray absorption spectroscopy (XAS) is a powerful experimental method for investigating the atomic and molecular structures of the catalytic and other nanoparticle materials [9].

Metal-supported materials find various applications (from preparation of fine chemicals to destruction of VOCs) in catalysis and with recent developments in nanoparticles approaches, modified nano-sized active metal particles are becoming of new interests in metal-supported catalysis. Highly dispersed nano-metal particles with high surface free energy have unique structural and electronic properties. Compared to large metal particles, the morphology and electronic (short-range ordering, valence band) properties of metal nanoparticles are fundamentally different. The interaction(s) between nanoparticles and supports significantly influences the unique properties of metal nanoparticles. Thus, designing of best catalysts is becoming more reliant on gaining the exact information about the structure and nature of the active metal catalytic sites.

Gold particles <15 nm exhibit unique activity at room temperature due to a meta-stable interatomic bonding of gold atoms. Catalyst containing nano-gold particles has three main features: fast reaction rate, high selectivity, and low reaction temperature [10]. Nano-gold catalyst has a great capability of oxidizing carbon monoxide at room temperature. For the catalyst to be active the gold particle size should be less than 5 nm and the metal–support interaction between the gold and its support must be strong. The preferred supports are the p-type and n-type semiconductor metal oxides, such as oxides of Ti, Fe, Co, and Ni, etc. The nano-gold supported metal (Al/Zn/Fe/Co/Ni) oxide materials are used as a catalyst in some selective oxidation reactions of hydrocarbons and the oxidation of carbon monoxide at room temperature. The examples of selective oxidation reaction of hydrocarbons include preparation of an alcohol from an alkane, an epoxide from an alkene, and a hydroxyl aromatic hydrocarbon from an aromatic hydrocarbon.

Gold nano particle containing supported metal oxide materials are normally used as catalyst or adsorbents. High purity iron, cobalt, manganese, and cerium oxide materials containing various loading of gold nanoparticles were prepared. These materials were chosen because they provide, especially due to their characteristic semiconductor properties, better metal–support interaction, and high surface area and may act as active co-catalyst or inert support materials. The main aim of the research project was to investigate the properties of gold nanoparticles supported on different iron, cobalt, manganese, and cerium oxide materials. Sophisticated techniques, such as X-ray absorption fine structure (XAFS), in situ high temperature XRD, and Mössbauer spectroscopy were employed to evaluate the characteristic behaviour of gold nanoparticles in various materials under different treatment conditions.

2. Experimental

The precipitation–deposition/co-precipitation methods [11,12] were used to synthesize the gold nanoparticle materials. Gold nanoparticles were supported on the oxides of iron, cobalt, manganese, and cerium using the above-mentioned methods. The gold nanoparticle containing materials were prepared by simultaneous precipitation of gold and metal oxide using dilute sodium hydroxide/sodium carbonate under an inert atmosphere/by immersing the calcined material in dilute $HAuCl_4$ (<0.2 g/L) solution at 328 K for 7 h (with continuous stirring) and precipitating gold hydroxide using NaOH. After the completion of the preparation process, the precursor is washed, dried at 323 K for 14 h, and calcined at 643 K for 5 h in helium. During the sample preparation, the gold precursor is deposited into the macro pores of the material and precipitated as gold hydroxide. Upon further heating the sample at 643 K, gold hydroxide is reduced to metallic gold. For studying the influence of high temperatures above 800 K on the properties of gold nanoparticles, the as-prepared Au-Fe_2O_3 (a) (Table 1) sample was heated at different temperatures (313, 573, 873, and 1273 K) in an inert-helium atmosphere.

The chemicals used in the synthesis of the materials were high purity salts (nitrate/chloride) of iron, cobalt, manganese, and cerium (Aldrich), sodium hydroxide (BDH), and water based gold chloride solution. The materials were characterized for their chemical composition, phase purity, structure, surface properties, and particle size using standard and sophisticated instrumental techniques, such as ICP-MS (HP4500 Series 300), XRD (Bruker D8 Advance), BET, TEM (JEOL 2010 at 100 kV), TGA, respectively. The surface area and total-pore volume of the materials were obtained by N_2-dynamic adsorption/desorption technique ($p/p_o = 0.3$) using a Micromeritics ASAP2000 Instrument. The details of instruments utilized and characterization methods are reported elsewhere [13–15].

Au L_3-edge EXAFS spectra were recorded in fluorescence mode at the Australian National Beamline Facility (ANBF), Beamline 20B (bending magnet) (2.5 GeV Photon Factory, KEK, Tsukuba, Japan). The excitation energy was selected using water-cooled Si(1 1 1) channel cut crystal monochromator (11 m away from the light source). The beam size of 2 mm (horizontal) × 1 mm (vertical) was controlled with a slit assembly (13 m away from the source). Using an Au foil as an internal standard performed energy calibration

Table 1
Chemical composition of gold nanoparticles supported on different metal oxide materials

Material type	Product composition (mol%)		Me/Au
	Au	Me	
Au-Fe	1.816	98.184	54.1
Au-Co	1.2	98.8	82.3
Au-Mn	1.25	98.75	79
Au-Ce	1.22	98.78	81

and the energy reproducibility was checked from time-to-time. Fluorescence was measured using a Canberra GL0110S 10-element Ge array detector. The signal from each array element was passed from the detector, via a Canberra Model 2026XA Spectroscopy Amplifier (shaping time, 0.25 μs), to a Canberra Model 2030 Single Channel Analyzer, which was set to pass the Au L_3-edge signal to the counting electronics. For all samples, 4/5 scans (scan time, ∼60 min) were taken at the energy range: 11,800–12,800 eV. The fluorescence was normalized to the incident beam flux monitored by an ionization chamber with a 30-cm path length containing standard Ar/Kr mixtures.

The spectra were recorded (in fluorescence mode) at room temperature. Powder samples were pressed into (<0.5 mm thick) pellets supported in an aluminium spacer between Kapton tape windows. The spectra were averaged from 4/5 scans. Averaging, background subtraction, random errors (arising due to noise) and calculation of theoretical EXAFS spectra were performed using the XFIT software package. The model fitting calculations were performed using the XFIT program, where a non-linear least squares procedure is used to fit the model parameters to the observed XAFS [16,17]. XFIT incorporates ab initio calculations of the XAFS using the programs FEFF 4.06 for single scattering and FEFF 6.01 for multiple scattering. The parameters, such as coordinates of all atoms, Debye-Waller factors, threshold energy, etc. were varied to optimise agreement between the calculated and observed XAFS. The observed and calculated XAFS were Fourier filtered and the goodness-of-fit parameter and statistical errors were estimated according to the reported methods [16]. The entire chi function was fit. For EXAFS measurements, as prepared (Au-Fe), calcined (Au-Fe, Au-Co, Au-Mn, Au-Ce oxides) and heated treated (Au-Fe at 573, 823, and 1273 K) samples were used.

^{197}Au Mössbauer spectra were measured on a Wissel Mössbauer spectrometer system consisting of an MDU-1200 function generator; DFG-1200 driving unit, MVT-100 velocity transducer and MVC-1200 laser calibrator (Toho University, Tokyo, Japan). Both the Mössbauer source and the absorber were kept at 12 K in a cryostat incorporating a closed cycle refrigerator, and the gamma rays were counted with a pure germanium solid-state detector. Mössbauer source (360 MBq) was prepared by neutron irradiation of a 100 mg disc of enriched metallic ^{196}Pt in the JRR-4 reactor of JAERI. The absorber thickness was about 80 mg Au cm^{-2}. The data were analyzed by the usual least squares method. The isomer shift is given relative to ^{197}Pt/Pt source at 12 K. The samples studied were Au-Fe, Au-Co, and Au-Mn oxides under different conditions. The study of very small metal atom clusters offers interesting insights into the transitional regime between atomic, molecular, and solid state physics. Mössbauer spectroscopy is a useful tool in the investigation of gold particles as it can furnish information on the s-electron density at the gold nuclei from the IS and on the symmetry of the environment of the gold atoms from quadrupole splitting (QS) [18].

In situ high temperature X-ray analysis was performed on Au-Co and Au-Mn samples from 323 to 1673 K using a Bruker D8 Advance XRD (using a Ni-α filtered Cu Kα X-ray source) with in situ high temperature (HTK2000) attachment. In situ high temperature XRD experiments were conducted under vacuum.

3. Results and discussion

The gold nanoparticles containing materials and their chemical composition are given in Table 1. The chemical analysis of the samples showed that the concentration of gold varied (range 0.5–3.5 Au wt.%) with the metal oxide host structures. Fig. 1 shows the XRD patterns of the nano-gold materials. The XRD analysis confirmed the desired structure and phase purity of the iron (Fe_2O_3), cobalt (Co_3O_4), manganese (MnO_2/Mn_3O_4), and cerium (CeO) samples and the presence of gold (fcc) in these materials.

Investigation of the surface characteristics (surface area, pore volume, adsorption/desorption isotherm, pore size, and volume distribution) of the gold containing samples (Table 2) suggested their well-defined macro-porous nature. TEM analysis (Fig. 2) of the gold loaded materials showed the presence of gold in nanoparticulate form, with average nanoparticle size ranging between ∼3 and 5 nm (varying from sample to sample) and the high temperature treatments caused on increase in the gold particle size of 7 nm. The details of gold particle sizes are presented in Table 2.

The gold nanoparticles on various metal oxide material (as-prepared: Au-Fe (Fe/Au 54.1); Au-Co (Co/Au 82.3); Au-Mn (Mn/Au 79); Au-Ce (Ce/Au 81)) were investigated for Au L_3-XAFS in order to elucidate variations in the local environment and structure around the gold atom. EXAFS data for the materials were obtained for at RT using the ANBF's experimental set-up. X-ray absorption spectra of gold nanoparticles on different metal oxide (Fig. 3; Table 1) materials exhibits slight difference in the peak height and fineness in features with the difference being more prominent in Au-Fe. The

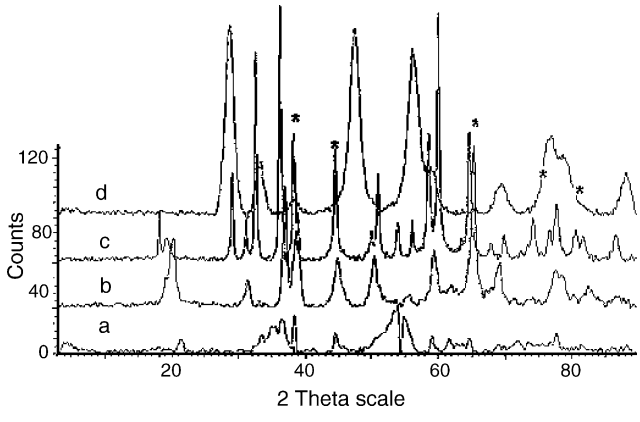

Fig. 1. X-ray powder diffraction patterns of the gold nanoparticles supported on different materials: gold nanoparticles on (a) iron oxide, (b) cobalt oxide, (c) manganese oxide, and (d) cerium oxide.

Table 2
Particle size and surface characteristics of the gold nanoparticles supported on different metal oxide materials

Material type	Gold particle size (on as-prepared samples, nm)	Surface properties		Total pore volume (cm^3/g)
		Surface area (m^2/g)	Micropore volume (cm^3/g)	
Au-Fe (a)	3–5	43	0.003	0.19
Au-Co (b)	∼4	63	0.001	0.21
Au-Mn (c)	∼3	54	0.001	0.20
Au-Ce (d)	∼4–5	49	0.002	0.195
Au-Fe, 573 K (a1)	∼3–5	44	0.003	0.19
Au-Fe, 873 K (a2)	∼6	34	0.002	0.16
Au-Fe, 1273 K (a3)	∼7	17	0.002	0.12

XAFS spectra (Au L_3-edge) of these materials were moreover similar to that of metallic gold [19]. Usually the shorter bond length observed in smaller nanoparticles is due to the lower coordination number and asymmetric distribution of Au (the near-neighbour Au-Au distribution).

Figs. 3 and 4 show the experimental (solid black lines) and theoretical (calculated best fits) (dotted lines) plots of the Au L_3-edge k^3-weighted EXAFS function k^3c (k) and Fourier transform of Au-Fe/Au-Co/Au-Mn/Au-Ce samples. For all the samples, the goodness-of-fit value (R) was in the range 16–20% (Table 3) and the value of the energy E in the fitting procedure varied from −3.5 to −8.5 eV.

The XAFS (Fig. 3) and Fourier transforms (Fig. 4) show the presence of a few oxidic gold (Au-O) and most of the metallic gold species (Au-Au) (Au-M support). The similarity of XANES and Fourier transforms in various metal oxide materials (Fe/Co/Mn/Ce) with different gold concentration indicates the local structure around the gold atom is similar despite the elements in the material. However, in the case of the Au-Co, the signals observed between 1.2 and 2.0 Å and 3 and 4.5 Å are more prominent than the Au-Fe, Au-Mn, and Au-Ce materials. On the radial distribution curve, the characteristic profile of metallic gold is easily recognized (Au-Au ∼2.72 ± 0.02 Å). A signal at about 1.6–1.8 Å observed in the radial distribution curve is characteristic of oxidized gold surrounded by light atoms (mostly short Au-O bond).

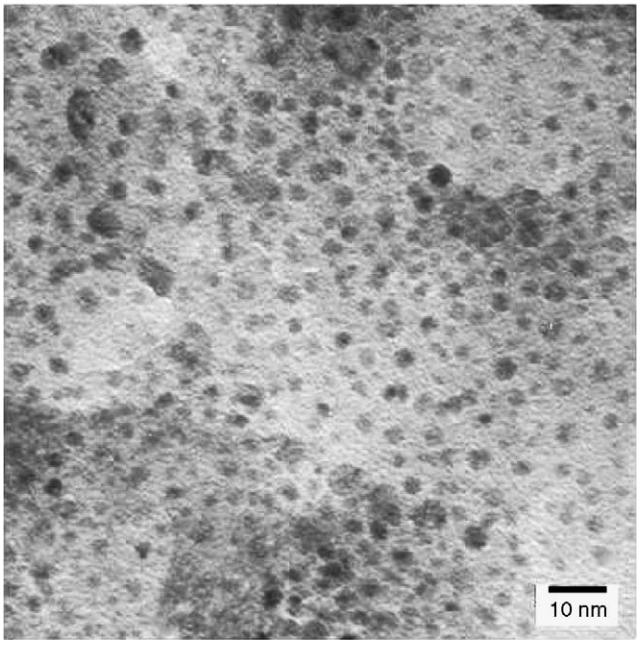

Fig. 2. TEM of the Au-Fe catalyst.

The bond length and other parameters (Debye-Waller factor and R factor) results obtained from EXAFS analysis are summarized in Table 3. The signal around 2.2 ± 0.5 Å observed in certain samples can be assigned to the binding of Au with the Cl or Au or O or support element (designated as M) (depending upon the treatment conditions and support type) [12,20]. The observed signal at 2.18 Å in the Au-Fe (a) sample is related to the binding of Au with Cl, while in the high temperature treated Au-Co (b), Au-Mn (c), and Au-Ce (d) samples the signal at ∼2.14 Å is related to the binding of Au with Au/O/support (M) [19]. In the Au-Fe (a1) sample, which was heated at lower temperature (573 K), the observed signal at 2.20 Å is related to the binding of Au with Cl while the signal observed at ∼2.11 Å, in the high temperature calcined gold–iron samples (Au-Fe, 873 K (a2) and Au-Fe, 1273 K (a3)) is related to the binding of Au to the support element (Fe). The Au-Fe/Co/Mn/Ce materials mostly show three to four types of coordination number.

The magnitude of Au-Au and Au-M peaks as well as their relative ratios in radial distribution function slightly varied in different host iron, cobalt, and manganese, and cerium oxide materials. The observed low Au-Au signal at ∼2.72 ± 0.02 Å indicates the presence of small gold particles [19,20]. In the bulk gold foil, the Au-Au signal was observed at 2.85 Å. The XRD measurements on the gold nanoparticles in the metal oxide materials indicated a face centred cube structure.

Figs. 5 and 6 show the experimental (solid black lines) and theoretical (calculated best fits) (dotted lines) plots of the Au L_3-edge k^3-weighted EXAFS function k^3c (k) and Fourier transform of Au-Fe samples calcined at different temperatures ((a) 313, (b) 573, (c) 873, and (d) 1273 K). The treatment temperatures exhibited changes in the feature of XAFS spectra and the peak height. The BET analysis of the thermally treated Au-Fe (a1) sample at 573 K exhibited ∼10% reduction in the surface area while at 873 K and 1273 K, the surface area of the Au-Fe catalyst was reduced by 30.9% and 65%, respectively.

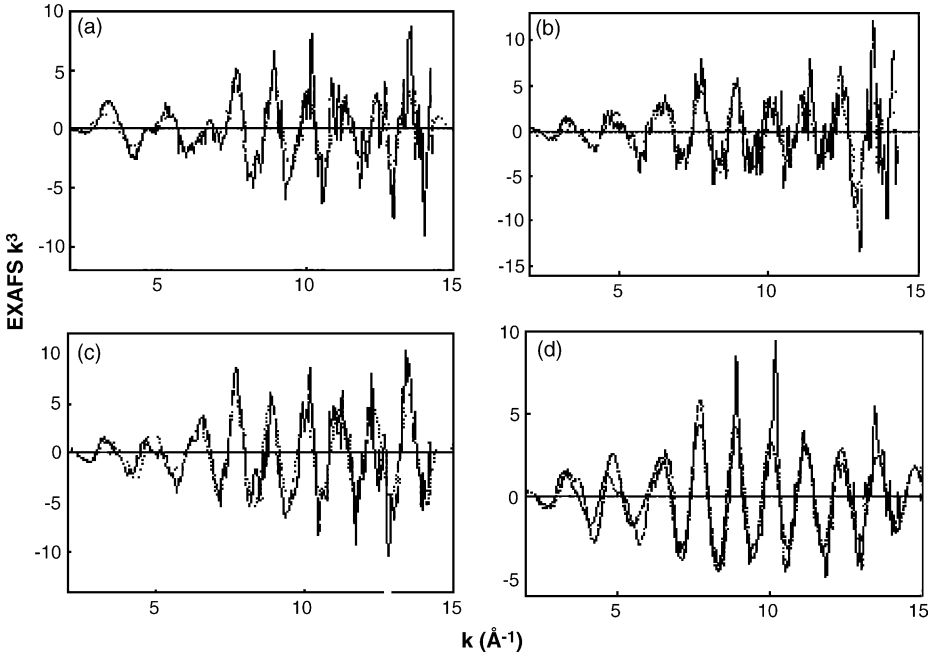

Fig. 3. EXAFS spectrum (Au L_3) of gold nanoparticles on: (a) iron oxide (a2), (b) cobalt oxide, (c) manganese oxide, and (d) cerium oxide. The solid lines are experimental data, and the overlaid dotted lines are the best fits (calculated).

The Au L_3-edge *k*-weighted EXAFS function *kc* (*k*) along with best fits (*R* factors in range of 16–20%) and corresponding radial distribution curves of as-prepared and thermally treated Au-Fe samples are shown in Figs. 4 and 5. The high treatment temperature significantly affects the magnitude of Au-O, Au-M, and Au-Au and their ratios. The as-prepared Au-Fe sample shows mostly the presence of Au-O species, however, with the increase in the temperature (above 573 K), significant changes in the Au species (the magnitude of Au-O, Au-M, and Au-Au and their ratios and peak width (Fig. 6)) were observed. The high temperature (above 873 K, 1273 K) treated Au-Fe (a2 and a3) samples showed minor changes in

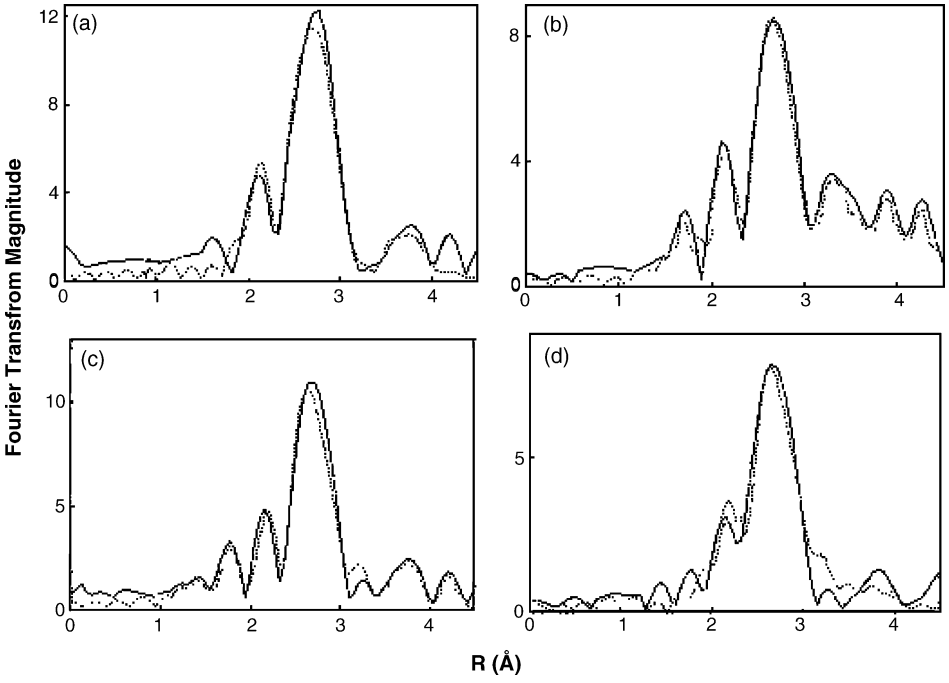

Fig. 4. EXAFS Fourier transforms (AuL_3) of gold nanoparticles on: (a) iron oxide, (b) cobalt oxide, (c) manganese oxide, and (d) cerium oxide. The solid lines are experimental data, and the overlaid dotted lines are the best fits (calculated).

Table 3
Data of the atomic distances, Debye-Waller factor, and *R* factor of gold nanoparticles supported on different metal oxide materials

Material type	Atom type	Bond length (Å)	Debye-Waller factor (Å^2)	*R* factor (%)	Symmetry
Au-Fe (a)	O-Mj	1.57	0.0027(1)	21.1	
	Cl sh	2.18	0.001		
	Au[a]	2.61	0.003		
Au-Co (b)	O	1.75	0.0038(1)	18.5	fcc
	Au/M	2.14	0.0042(1)		
	Au	2.72	0.0034(2)		
Au-Mn (c)	O	1.8	0.004(2)	17.5	fcc
	Au/M	2.16	0.005(1)		
	Au	2.73	0.0024(2)		
Au-Ce (d)	O	1.77	0.003(1)	16.8	fcc
	Au/M	2.14	0.004		
	Au	2.72	0.006		
Au-Fe, 573 K (a1)	O	1.58	0.0018(1)	20.04	fcc
	O	1.88	0.003		
	Cl	2.20	0.0016		
	Au	2.73	0.0042		
Au-Fe, 873 K (a2)	O[a]	1.63	0.005(1)	19.5	fcc
	Au/M	2.12	0.0036(3)		
	Au	2.74	0.005(2)		
Au-Fe, 1273 K (a3)	Au/M	2.11	0.0049(1)	18.2	fcc
	Au	2.75	0.0075(1)		

(M = O/Cl/Me) A_i = Debye-Waller factor (Å^2) of the *i*th shell.
[a] Minor shoulder peak.

the feature of XAFS spectra but the peak height was noticeable. In case of the Au-Fe (a3) sample (treated at 1273 K), no peak related to the oxidic gold species was observed which indicated the transformation of oxidic gold species to Au-Au at higher temperature.

Table 3 shows the atomic distances and Debye-Waller factor and *R* factor parameters in the thermally treated Au-Fe material at 323, 573, 873, and 1273 K. The changes in bond lengths of Au were observed due to the thermal treatments at 873 and 1273 K. TEM measurement showed that the gold

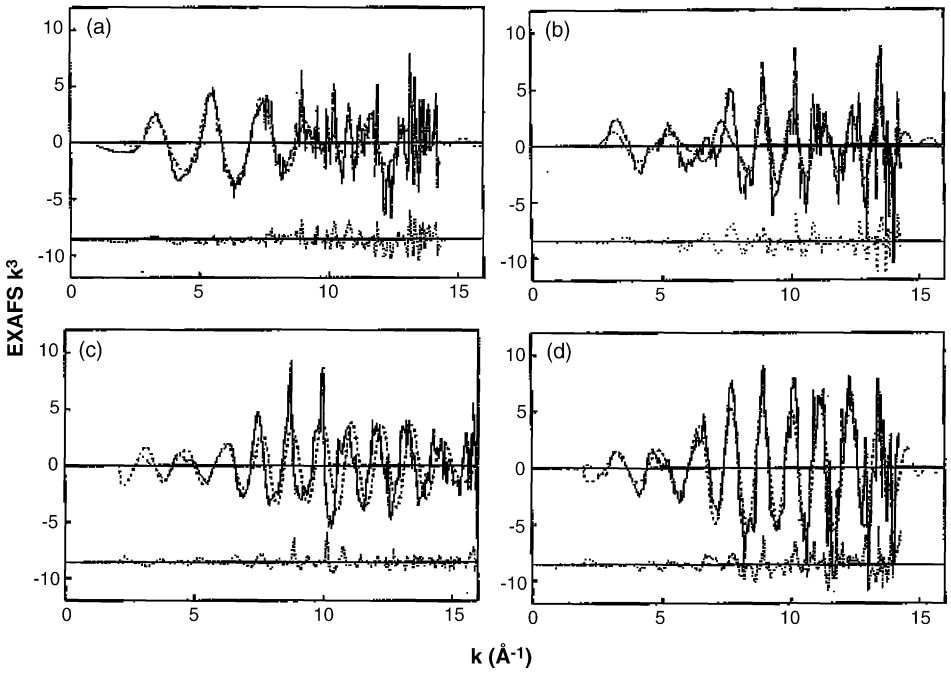

Fig. 5. EXAFS spectrum (Au L_3) of gold nanoparticles on iron oxide: (a) as-prepared; (b) calcined at 573 K; (c) calcined at 873 K; and (d) calcined at 1273 K. The solid lines are experimental data, and the overlaid dotted lines are the best fits (calculated).

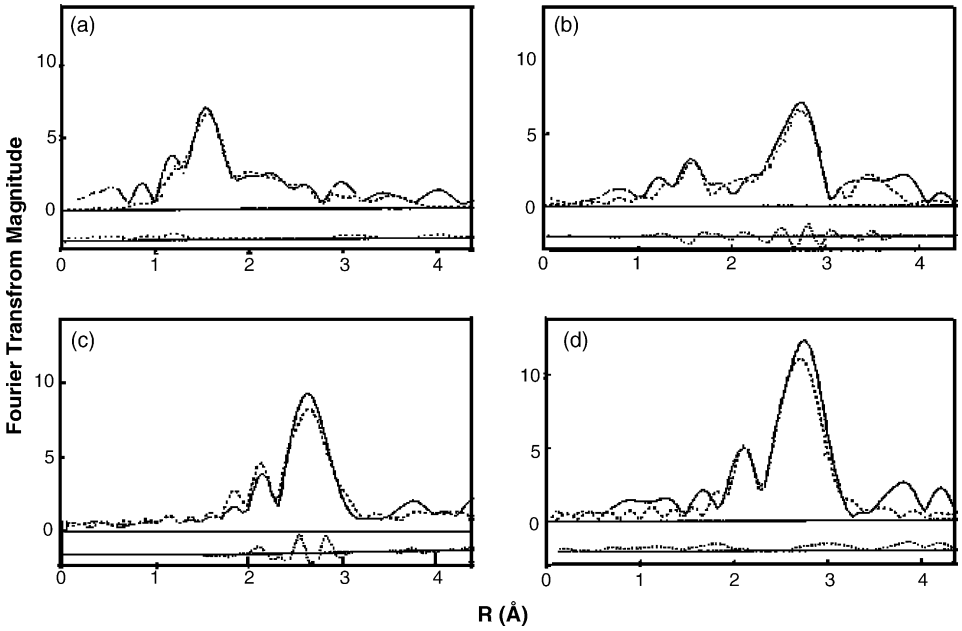

Fig. 6. EXAFS Fourier transforms (Au L_3) of gold nanoparticles on iron oxide: (a) as-prepared; (b) calcined at 573 K; (c) calcined at 873 K; and (d) calcined at 1273 K. The solid lines are experimental data, and the overlaid dotted lines are the best fits (calculated).

particle size increases up to certain levels with the treatment temperature (above 873 K). The increase in particle size is due to gold particle aggregation, which is quite significant at 1273 K. Fig. 7 shows the Au L_3-edge XANES spectra of gold nanoparticles on iron oxide, cobalt oxide, and manganese oxide, and cerium oxide samples. The site symmetry, spin state, atomic position of neighbours and oxidation state (edge shift–binding energy shift) of the metal are important information given by XANES. The XANES spectrum of the Au-Fe sample is different from the Au-Co, Au-Mn, and Au-Ce samples.

Fig. 8 shows Au L_3-edge XANES spectra of gold nanoparticles on iron oxide thermally treated at (a) 313, (b) 573, (c) 873, and (d) 1273 K. The XANES spectra were background corrected. In Fig. 7, the XANES data shows significant variations for the gold nanoparticles prepared using different support materials. The XANES clearly indicates oxidized as well as reduced Au species. Figs. 7 and 8 show four distinct edge features. In the "white line" peak (~11,928 eV) is suppressed in the XANES spectra of Au-Co, Au-Mn, and Au-Ce samples due to full occupancy of d states for gold. The peak around 11,940 eV is a weak feature but mostly present in bulk gold, gold nanoparticles, etc. while the two peaks between 11,940 and 11,980 eV are more structure dependent. The peaks after 11,940 eV represent the extended local structure around the absorbing atom [21].

It is interesting to note that the XANES spectrum (Fig. 7) for gold nanoparticles present in different metal oxide samples is different. The peaks in the 11,925–11,980 eV regions suggest that factors, such as the concentration of gold

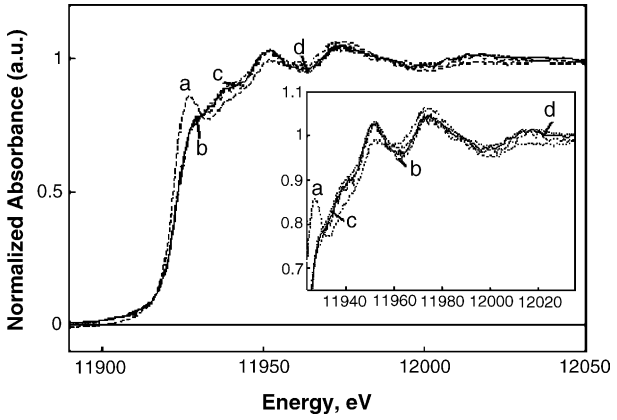

Fig. 7. Au L_3-edge XANES spectra of gold nanoparticles on: (a) iron oxide, (b) cobalt oxide, (c) manganese oxide, and (d) cerium oxide.

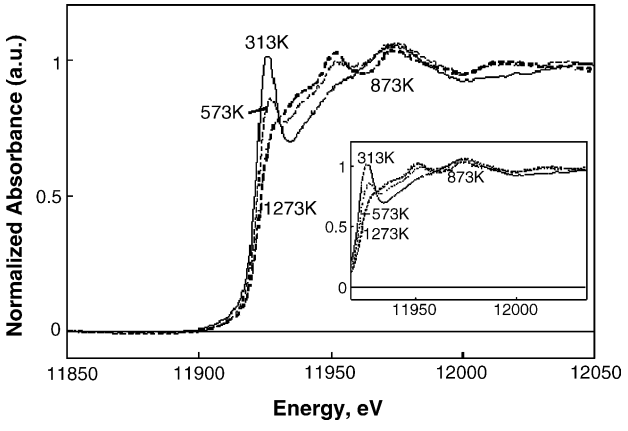

Fig. 8. Au L_3-edge XANES spectra of gold nanoparticles on iron oxide: (a) as-prepared; (b) calcined at 573 K; (c) calcined at 873 K; and (d) calcined at 1273 K.

nanoparticles and host element type structure influences the XANES.

Similarly, in the case of the thermally treated (313, 573, 873, 1273 K) gold nanoparticles (Au-Fe (a–a3)) materials, shifts in the peaks of XANES spectra (Fig. 8) were observed in the higher energy region. The XANES pattern of the heated treated Au-Fe samples is different than that of as-prepared Au-Fe (a) and Au-Fe sample calcined at 573 K. The Au-Fe samples treated at 313 K exhibits a strong peak at 11,926 eV and the intensity of this peak further decreases at 573 K. The 11,926 eV peak is not observed in the samples heated at 873 K and 1273 K. The Au-Fe sample treated at 313 K mostly contains Au-O species, which further gets converted to various Au-Au/Au-M species at higher temperatures. The intensity and width of these XANES peaks can be related [22,23] to the number of neighbours surrounding each gold atom as well as to the size of gold particle. In XANES spectra (Figs. 7 and 8) including XAS, the intense and defined peaks (in higher XANES region) are consistent with the reported results on gold nanoparticles [21].

The in situ high temperature XRD (HTXRD) patterns of gold nanoparticles in cobalt oxide and manganese dioxide structures are shown in Figs. 9 and 10. The in situ HTXRD measurements was undertaken to investigate the fate of gold nanoparticles and the influence of cobalt and manganese support structures on the containment of the nanoparticles at different temperatures (313–1673 K). The in situ HTXRD measurements on as-prepared Au-Co and Au-Mn were conducted in vacuum with a heating rate of 5 K/min and 1 h as a holding period for each temperature step.

In the case of the Au-Co material (Fig. 9), the in situ HTXRD results show that no major changes in the phases of gold and supports were observed up to a temperature of 523 K. However, above the temperature of 723 K, the cobalt support phase remained unchanged up to 1323 K and further changed above 1423 K. The gold peaks were observed up to a temperature of 1323 K and the intensity of gold peaks further significantly decreased above 1423 K. In case of the Au-Mn material (Fig. 10), the in situ HTXRD results showed that no changes in the phases of gold and Mn were observed up to 1423 K (except minor changes due to better crystallinity at high temperature). However, the Mn oxide phase-peak intensity decreased above 1523 K and a change in the phase was observed over 1673 K. The changes in the concentration of gold particles with the temperature are very interesting over the Co and Mn supports structures. From in situ HTXRD results, it is observed that substantial amount of gold particles, is easily retained within the cobalt and manganese materials over higher temperatures (∼1323 K).

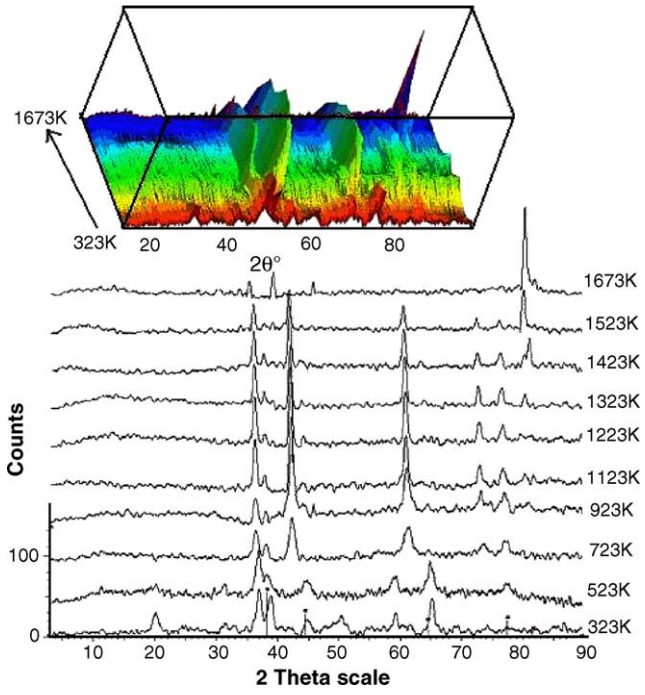

Fig. 9. In situ high temperature XRD analysis of gold nanoparticles on cobalt oxide material.

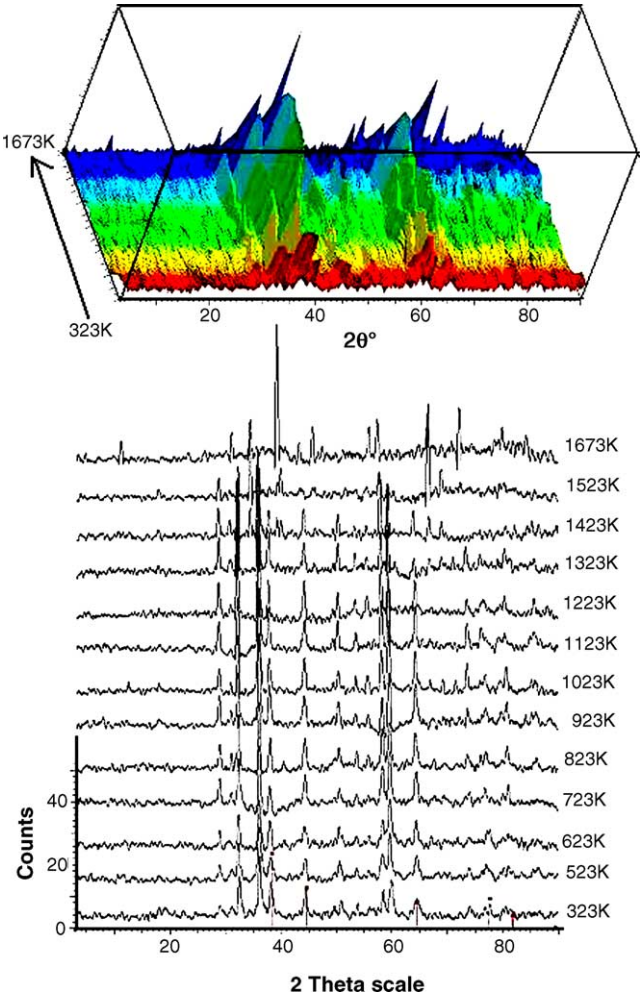

Fig. 10. In situ high temperature XRD analysis of gold nanoparticles on manganese oxide material.

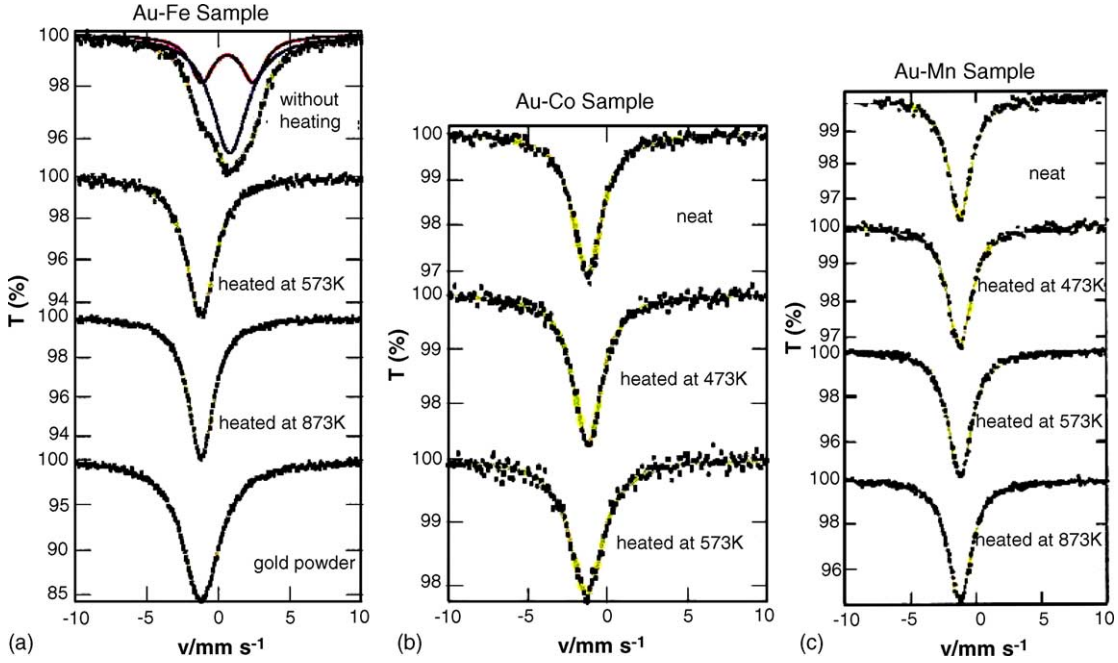

Fig. 11. ^{197}Au Mössbauer spectra for gold nanoparticles on: (a) iron oxide at 12 K, (b) cobalt oxide, and (c) manganese oxide.

^{197}Au Mössbauer spectra data have been reported and discussed for a variety of gold nanoparticles catalysts (supported Fe, Co, and Mn oxides). The ^{197}Au Mössbauer spectra obtained for gold nanoparticles in Fe, Co, and Mn oxides are presented in Fig. 11. The aim of the studies is to reveal differences in the electronic configurations of surface and bulk atoms by means of ^{197}Au Mössbauer spectroscopy. In Au-Fe, Au-Co, and Au-Mn samples, all ^{197}Au spectra (except the spectra of unheated Au-Fe sample) consist of mostly one to two components. The ^{197}Au spectrum unheated samples of Au-Co and Au-Mn consist of two components, major component, and minor components. Major component represents metallic gold, which gives rise to a single line with an isomer shift of 1.23 mm s^{-1}. The second minor component has a positive isomer shift and an unresolved quadrupole splitting.

In the case of the Au-Fe material, the ^{197}Au Mössbauer spectra obtained for gold nanoparticles (Fig. 11) shows different spectrum for the as-prepared Au-Fe and calcined materials. The spectrum for the as-prepared Au-Fe was fitted to three peaks with a single central peak bulk metallic Au core-atoms. A peak in the positive velocity side is due to Au^{3+} species [24] (according to the mean isomer shit and quadrupole splitting, this component represents trivalent gold as an oxidic phase [25]) while the shoulder on the negative velocity side is due to Au^{+} species. These Au species get converted to metallic gold species with increasing in the temperature (573–873 K) (Fig. 11). In the heated Au-Fe samples, Au^{3+} and Au^{+} species are reduced to metallic gold by heat-treating. In Au-Co and Au-Mn oxide samples, gold nano particles are mostly metallic gold form as shown by Mössbauer spectra in Fig. 11 and by heating the metallic gold becomes more and more predominant.

4. Conclusions

Gold nanoparticles with different size and concentration could be easily prepared in the medium to high surface area iron, cobalt, manganese, and cerium materials. The TEM results indicate that the dispersion and size of gold nanoparticles are different in the materials with Fe/Co/Mn/Ce supports. The nano-gold particles within these materials possess higher thermal stability. In situ HTXRD measurements on these materials showed that the gold nanoparticles are contained up to high temperatures in these materials.

On the Au-Fe, Co-Au, Au-Mn, and Au-Ce and high temperature treated Au-Fe oxide samples, the XAFS/XANES and Fourier Transform show the presence of few oxidic gold species with the majority of them being metallic gold species (either Au-Au or Au-Me). Variation in the magnitude of Au-O/Au-Au in the radial distribution function is also observed. The changes in the XAFS, XANES, and Mössbauer spectra suggest that various factors, such as the host support type (Fe/Co/Mn/Ce) and structure, particle size, metal concentration, and calcination temperature influences the characteristics of the nano-gold particles. The gold nanoparticles in different Fe/Co/Mn/Ce support structures exhibits different Au bond length and the Au-Au signal at $\sim 2.72 \pm 0.02$ Å indicates the presence of small gold nanoparticles. In the Au-Fe sample, the high treatment temperatures influence the magnitude of Au-O, Au-M/Au-Au, their ratios

and the transformation of oxidic gold species to Au-M or Au-Au.

Acknowledgments

We gratefully acknowledge the financial support of the Australian Synchrotron Research Program (Australian Nuclear Science and Technology Organization, ANSTO), Sydney. We thank ANBF (Australian National Beamline Facility, 20B) team, Photon Factory of the National Laboratory for High Energy Physics (KEK), Tsukuba, Japan for assistance and facility support.

References

[1] V.P. Zhdanov, B. Kasemo, Surf. Sci. Lett. 511 (2002) 23.
[2] V.V. Gorodetskii, W. Drachsel, Appl. Catal. A: Gen. 188 (1999) 267.
[3] T. Kobayashi, M. Haruta, S. Tsubota, H. Sano, Sens. Actuators B1 (1990) 222.
[4] M. Haruta, Catal. Today 36 (1997) 153.
[5] M. Haruta, Catal. Surv. Jpn. 1 (1997) 61.
[6] M. Haruta, N. Yamada, T. Kobayashi, S. Iijima, J. Catal. 115 (1989) 301.
[7] M. Haruta, T. Kobayashi, H. Sano, N. Yamada, Chem. Lett. 405 (1987).
[8] N.M. Gupta, A.K. Tripathi, J. Catal. 187 (1999) 343.
[9] D.C. Koningsberger, R. Prins, in: D.C. Koningsberger, R. Prins (Eds.), X-ray Absorption, Jonh Wiler & Sons, New York, 1988.
[10] K.-C. Wu, Y.-L. Tung, C.-C. Dai, United States Patent Application 20,040,127,353, July 1 (2004).
[11] S. Tsubota, M. Haruta, T. Kobayashi, A. Ueda, Y. Nakahara, G. Poncelet, al. et (Eds.), Preparation of Catalysts V, Elsevier Science B.V., 1991, p. 695.
[12] D.B. Akolekar, G. Foran, S.K. Bhargava, J. Synchrotron Radiat. 11 (3) (2004) 284.
[13] D.B. Akolekar, J. Catal. 143 (1993) 227.
[14] D.B. Akolekar, A. Chaffee, R.F. Howe, Zeolites 19 (1997) 359.
[15] D.B. Akolekar, S.K. Bhargava, Stud. Surf. Sci. Catal. 105 (1998) 755.
[16] P.J. Ellis, H.C. Freeman, J. Synchrotron Radiat. 2 (1995) 190.
[17] XFIT for Windows'95; Australian Synchrotron Research Program, Sydney, 1996.
[18] L. Stievano, S. Santucci, L. Lozzi, S. Calogero, F.E. Wagner, J. Non-Cryst. Solids 232–234 (1998) 644.
[19] D. Guillemot, M. Polisset-Thfoin, D. Bonnin, V.Y. Borovkov, 12th International Zeolite Conference Materials Research Society, USA, 1999, p. 2079.
[20] H. Kageyamma, T. Tsubota, N. Kamijo, M. Haruta, Jpn. J. Appl. Phys. 32 (Suppl. 32–2) (1993) 445.
[21] R.E. Benfield, V.M. Grandjean, Pugin Kroll R., T. Sawitowski, G. Schmid, J. Phys. Chem. B 105 (2001) 1961.
[22] G.N. Greaves, P.J. Durham, G. Diakun, P. Quinn, Nature 294 (1981) 139.
[23] D. Bazin, D. Sayers, J.J. Rehr, C. Mottet, J. Phys. Chem. 101 (1997) 5332.
[24] S. Tsubota, M. Haruta, Report of the Osaka National Research Institute No. 393, 1999, p. 36.
[25] F.E. Wagner, S. Gavagno, C. Milone, A.M. Visco, L. Stievano, S. Calogero, J. Chem. Soc., Faraday Trans. 93 (18) (1997) 3403.